# Supplementary Material

# High metal loaded Cu(I)N3 single-atom catalysts: superior methane conversion activity and selectivity under mild conditions

Hyesung Lee and Sang-Yup Lee[*]

Department of Chemical and Biomolecular Engineering, Yonsei University, Seoul 03722 Republic of Korea
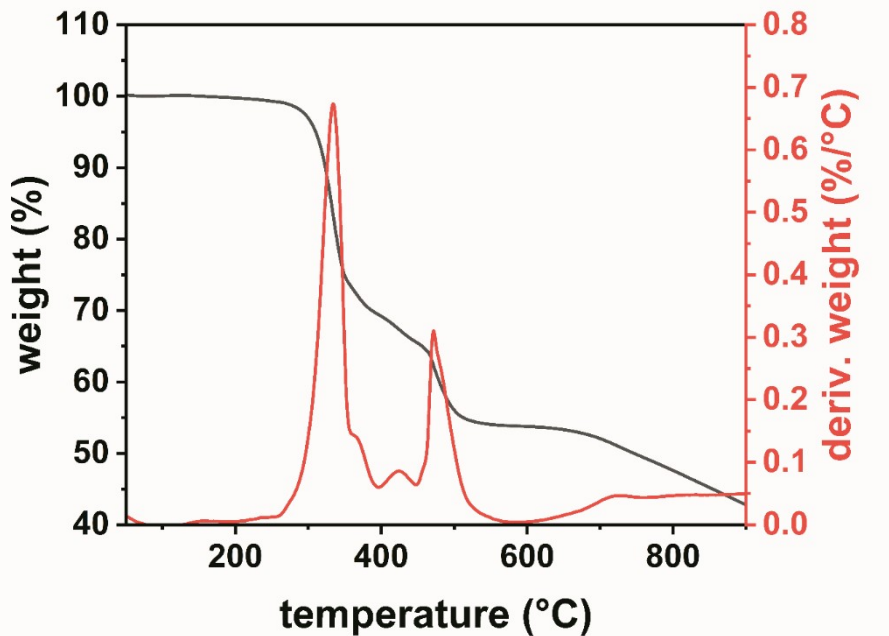
Figure S1. TGA and 1st derivation profiles of Cu(blm)$_2$.
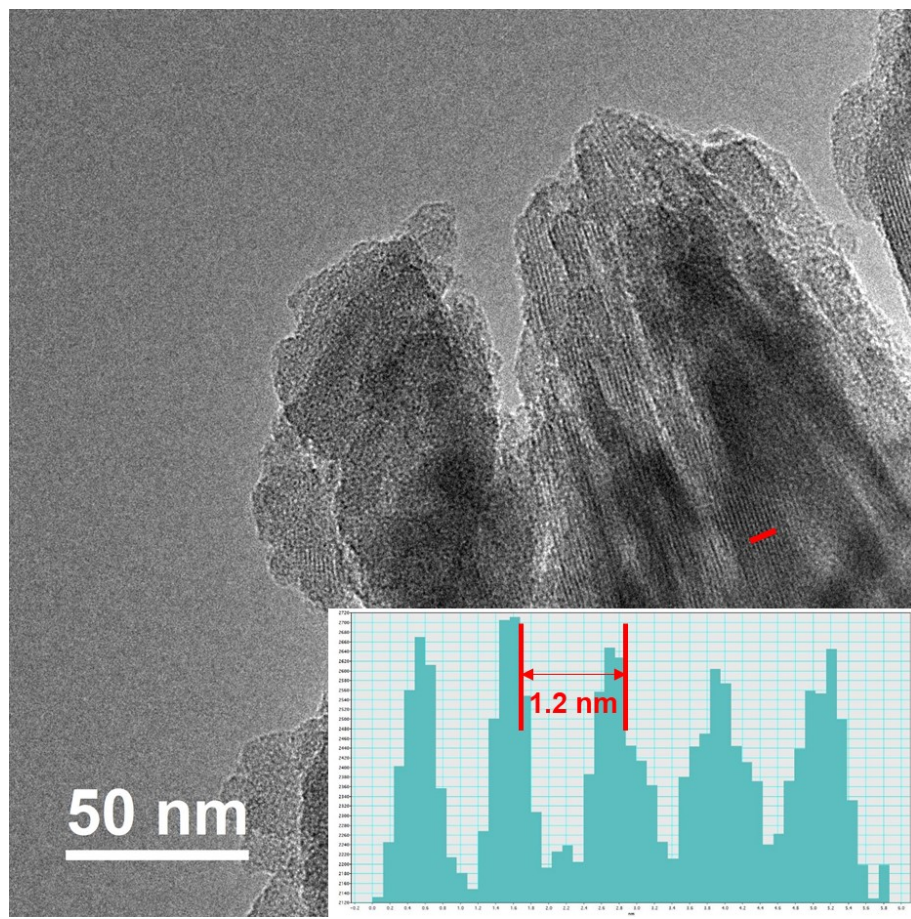
Figure S2. TEM image of the CuNC-600 showing carbon layers (inset: intensity profile of the region marked in red line).
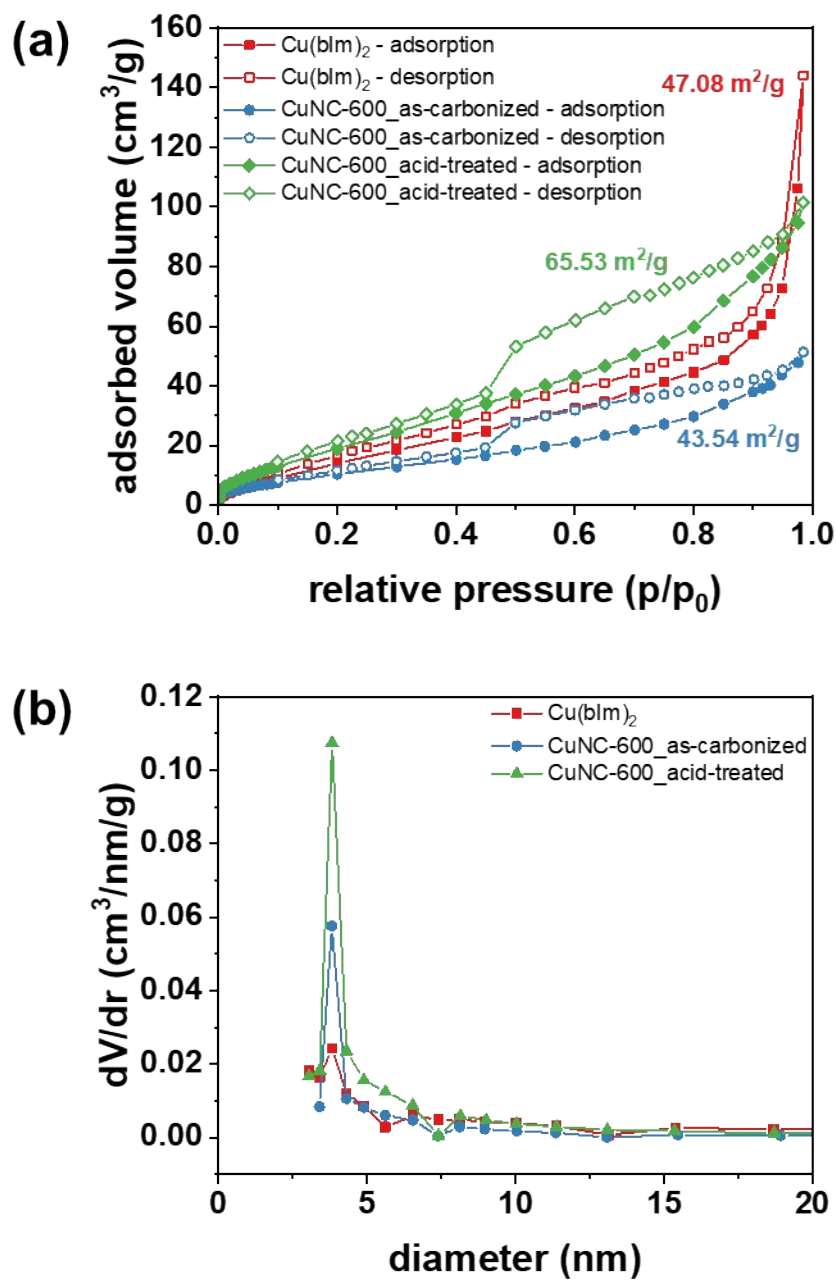
Figure S3. BET analyses of Cu(bIm)$_2$, as-carbonized and acid-treated CuNC-600. (a) N$_2$ isotherm at 77 K and (b) pore size distribution.
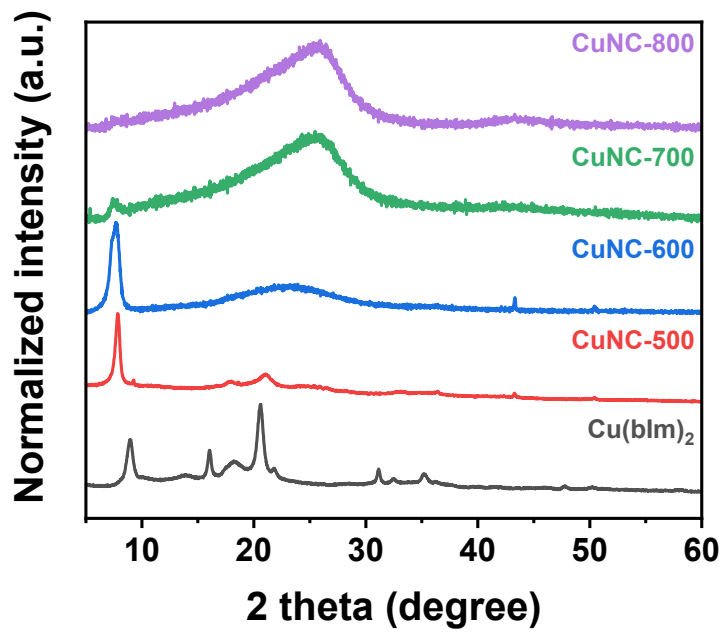
Figure S4. XRD patterns of Cu(bIm)$_2$ and CuNC catalysts carbonized at various temperatures.
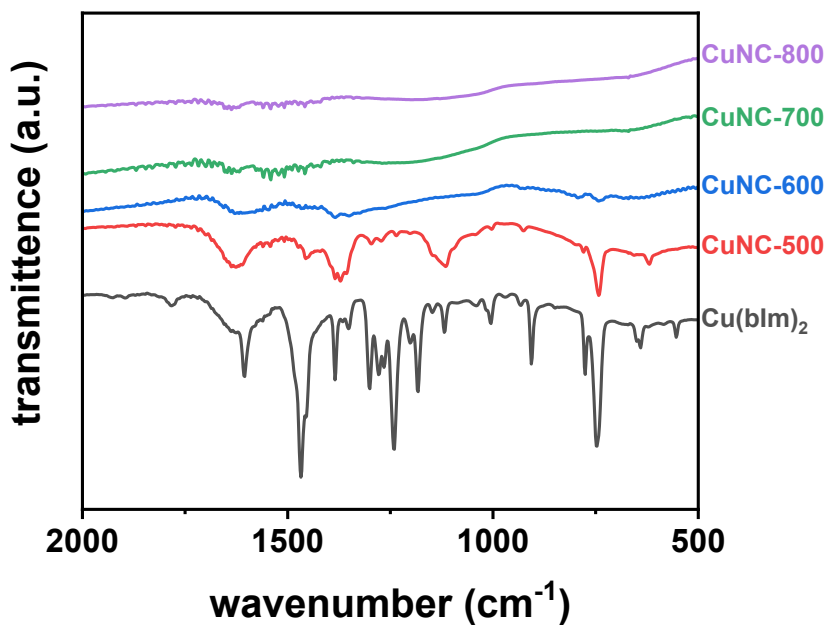
Figure S5. FT-IR spectra of Cu(bIm)$_2$ and CuNC catalysts carbonized at various temperatures.

Table S1. Wavenumbers and assignements of Raman and FT-IR peaks of Cu(bIm)$_2$.

FT-IR (cm^{-1})	Raman (cm^{-1})	Assignment
554	553	ring torsion
	583	
640	640	Imidazole ring torsion
650		
746		benzimidazole C-H out-of-plane bending
775	776	Imidazole plane ring bending
907		Benzimidazole in-plane ring bending
932		Benzimidazole in-plane ring bending
970		Imidazole C-H in-plane bending
1005		Benzimidazole in-plane ring bending
1016		Benzimidazole in-plane ring bending
1119		benzimidazole C-H out-of-plane bending
1148		Benzimidazole in-plane C-H bending
1182		Benzimidazole in-plane C-H bending
1202		Benzimidazole in-plane C-H bending
1240	1240	ring stretching
1265	1260	Benzimidazole in-plane bending
1279	1275	Benzimidazole in-plane bending
1300	1300	ring stretching
1350	1350	ring stretching
1385		ring stretching
1468	1466	ring stretching
1605	1609	ring stretching
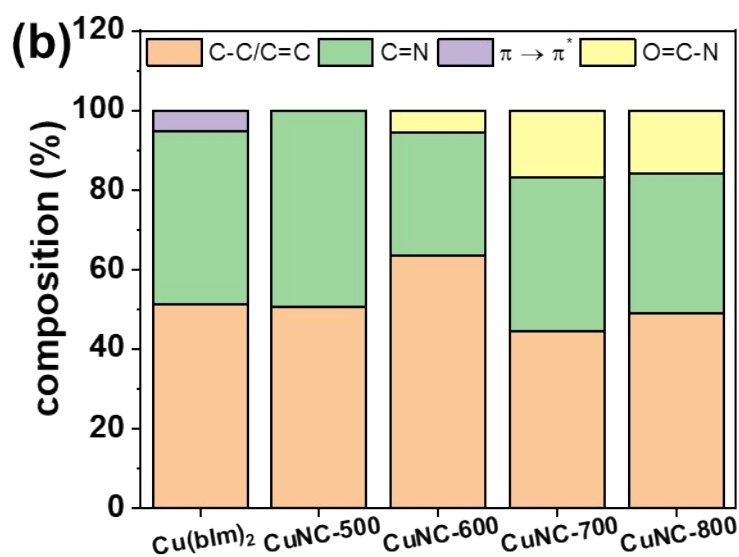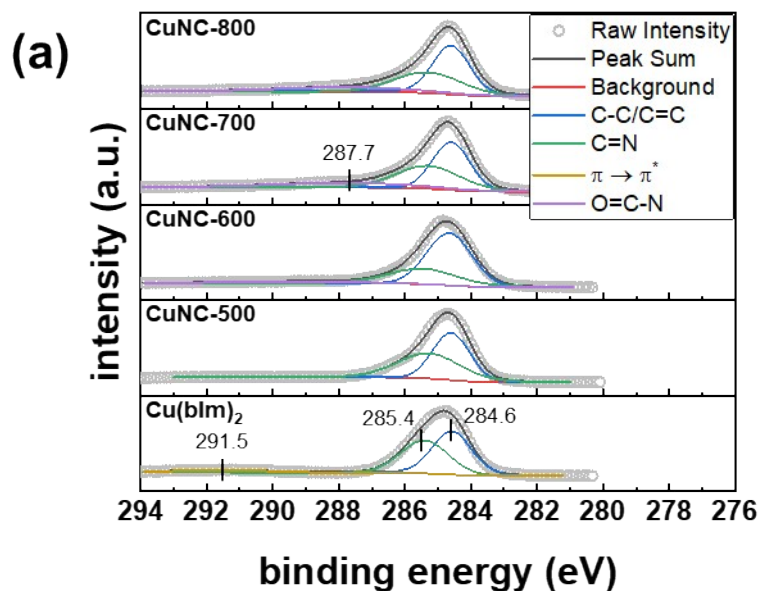
Figure S6. (a) High-resolution XPS C 1s spectra of Cu(bIm)$_2$ and CuNC catalysts, and the corresponding compositions of carbon species.

Table S2. Element analysis results determined by XPS analysis.

|	Elements (wt%)				
	C	**N**	**O**	**Cu**	**Sum**
Cu(blm)$_2$	55.7	17.2	1.9	25.2	100
CuNC-500	61.0	14.6	5.8	18.6	100
CuNC-600	61.1	14.9	6.3	17.7	100
CuNC-700	64.8	13.5	8.9	12.8	100
CuNC-800	69.4	10.6	9.0	11.0	100
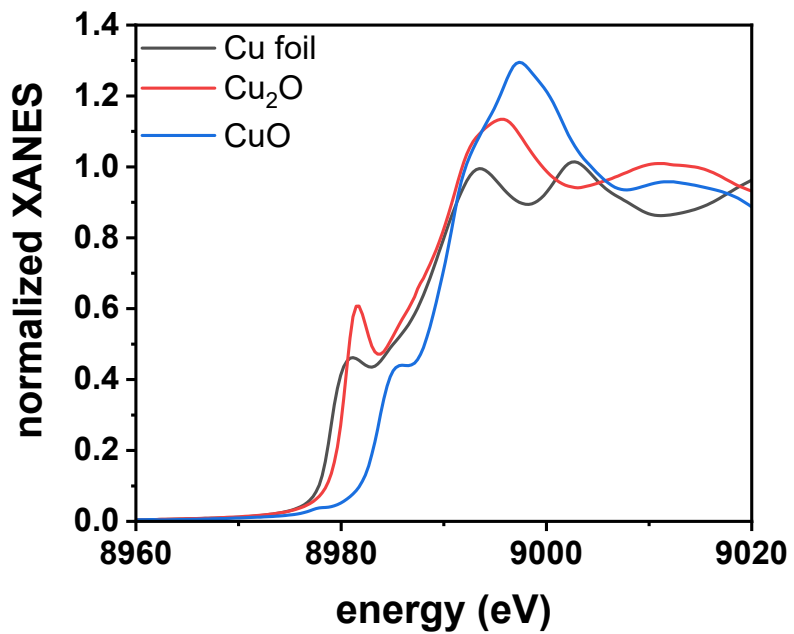
Figure S7. Cu-XANES spectra of Cu foil, Cu_2O, CuO.

Table S3. Detailed Cu-EXAFS fitting results of Cu(bIm)$_2$ and CuNC catalysts.

Catalyst	Path	Coordination number[a]	Distance (Å)	Debye-Waller Factor (Å^2)	R-Factor[b]
Cu(bIm)$_2$	Cu-N	4.22	1.97 (±0.006)	0.004 (±0.001)	
	Cu-C	8.44	2.99 (±0.02)	0.009 (±0.002)	0.007
	Cu-N-C	16.88	3.19 (±0.037)	0.017 (±0.007)	
CuNC-500	Cu-N	2.67	1.87 (±0.012)	0.005 (±0.002)	
	Cu-C	3	2.92 (±0.029)	0.004 (±0.003)	0.019
	Cu-C	2.67	3.18 (±0.046)	0.009 (±0.008)	
CuNC-600	Cu-N	2.77	1.91 (±0.010)	0.006 (±0.002)	
	Cu-C	1.84	3.16 (±0.060)	0.016 (±0.012)	0.003
	Cu-Cu	0.07	2.54 (±0.012)	0.007 (±0.004)	
CuNC-700	Cu-N	3.34	1.93 (±0.022)	0.008 (±0.003)	
	Cu-C	9.02	3.00 (±0.093)	0.020 (±0.016)	
	Cu-C-N	18.9	3.17 (±0.079)	0.016 (±0.015)	0.014
	Cu-Cu	0.35	2.56 (±0.063)	0.0077 (±0.0076)	
CuNC-800	Cu-N	3.79	1.95 (±0.014)	0.006 (±0.002)	
	Cu-C	3.67	3.05 (±0.055)	0.010 (±0.008)	
	Cu-Cu	0.6	2.54 (±0.020)	0.003 (±0.002)	0.019
	Cu-C	11	3.40 (±0.039)	0.018 (±0.005)	

[a]The error was within 20%. [b]a measure of the mean square sum of the misfit at each data point. Fit range: 2 < k < 11 Å^{-1}; 1 < R < 3 Å; Fit window: Hanning
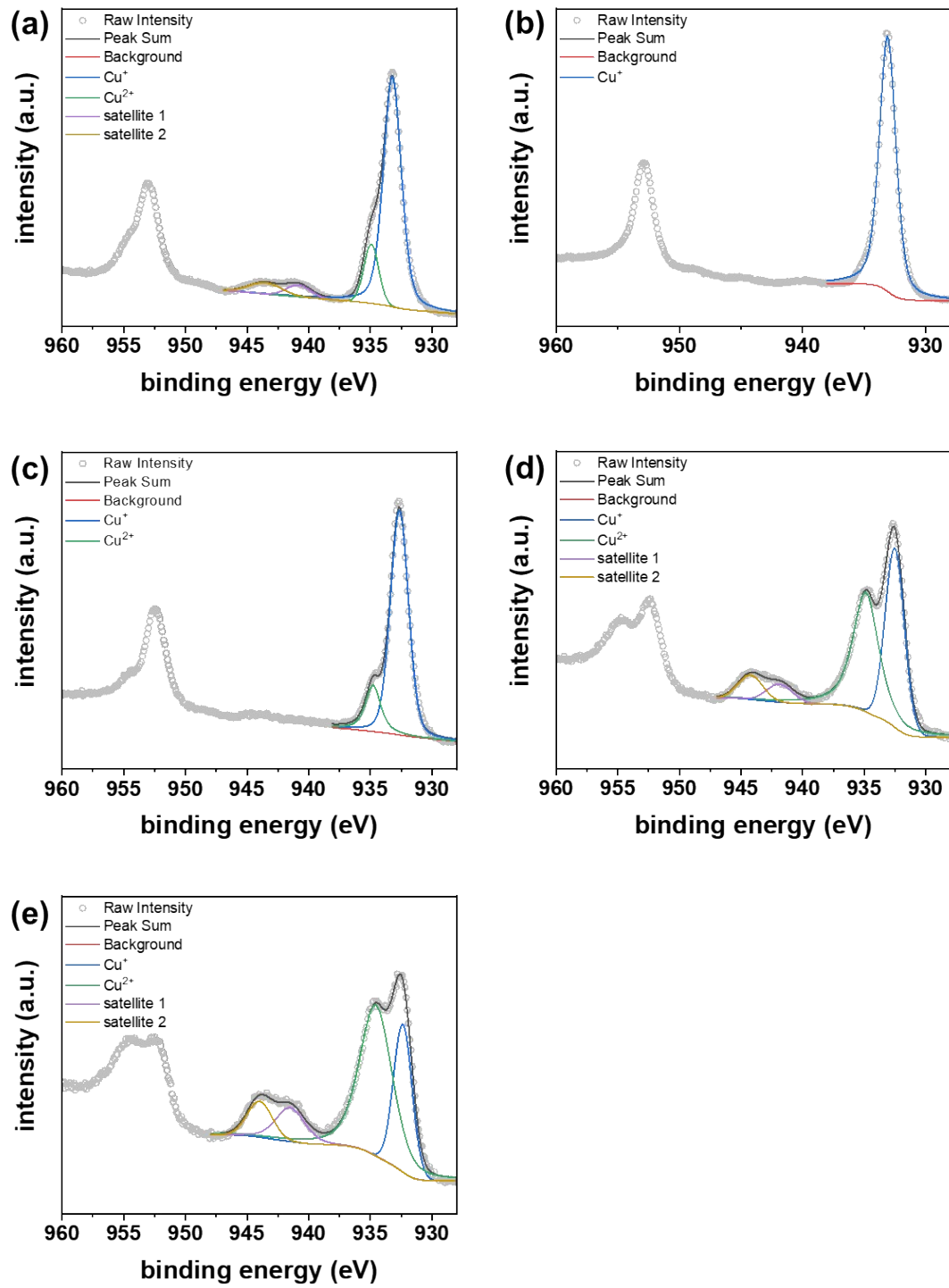
**Figure S8.** High-resolution Cu 2p XPS spectra of (a) Cu(bIm)2, (b-e) CuNC-500, -600, -700, and -800, respectively.
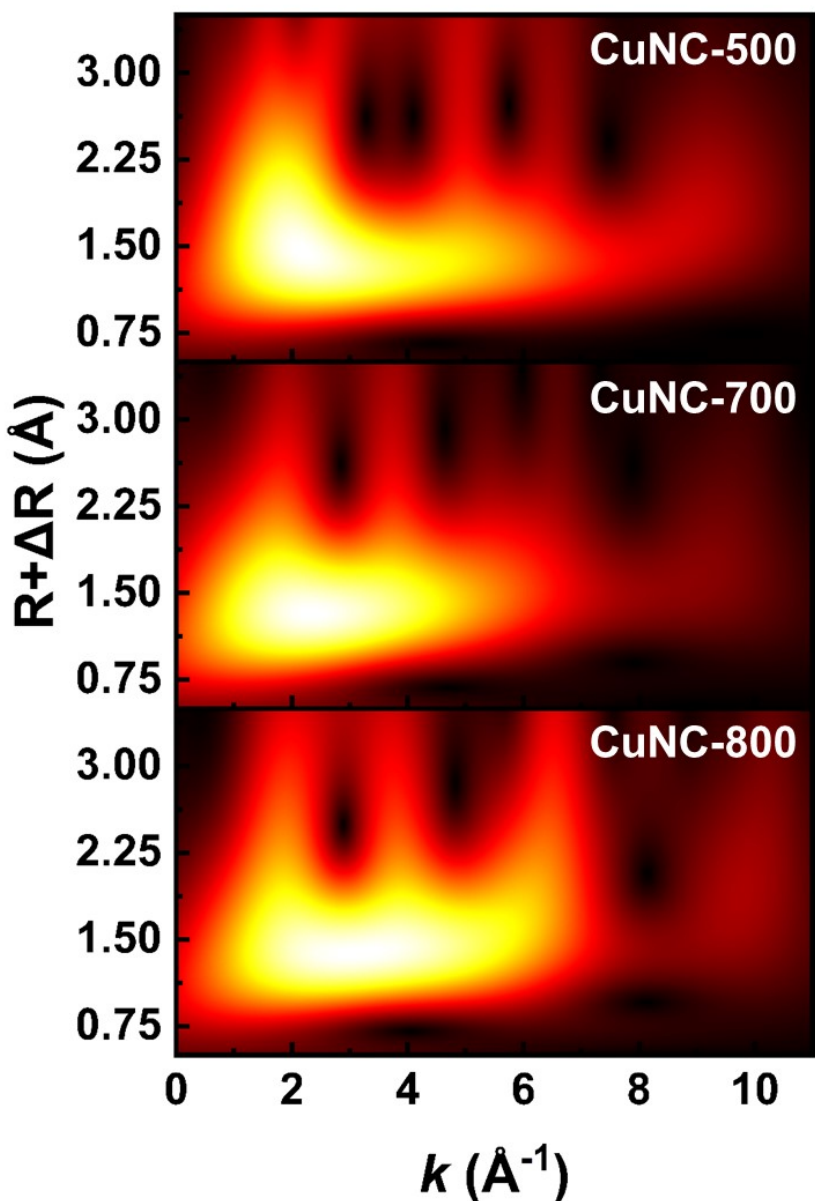
Figure S9. WT-EXAFS contour plots of CuNC-500, -700, and -800.
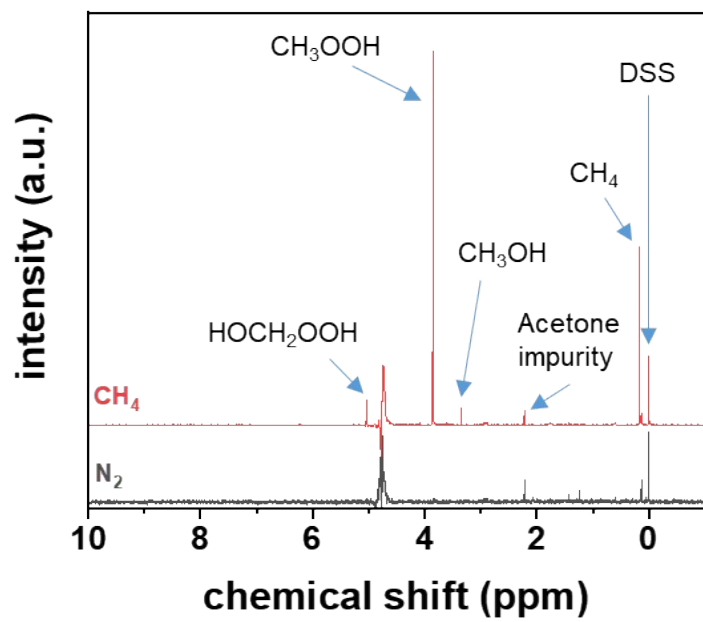
**Figure S10.** Typical 1H-NMR spectra of the product solutions using (a) CH_4 and (b) N_2.
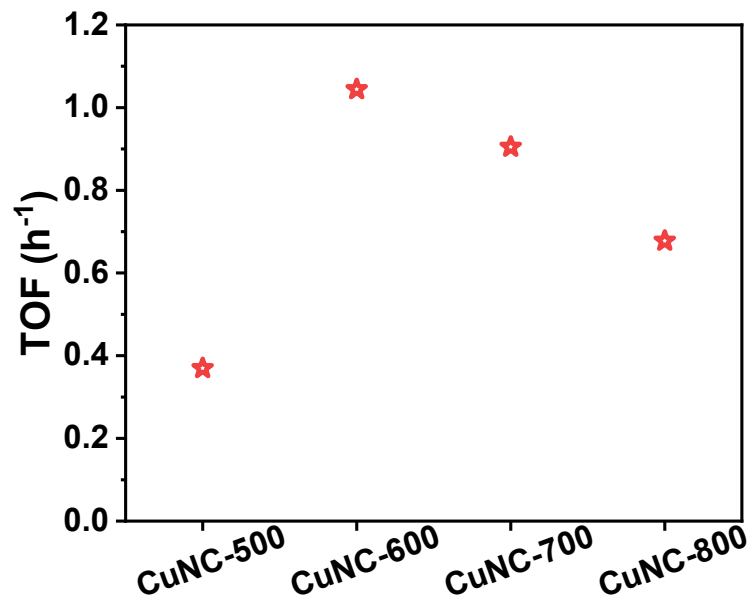
Figure S11. Turnover frequency (TOF) of C1 liquid products using $Cu(bIm)_2$ and CuNC-T catalysts.
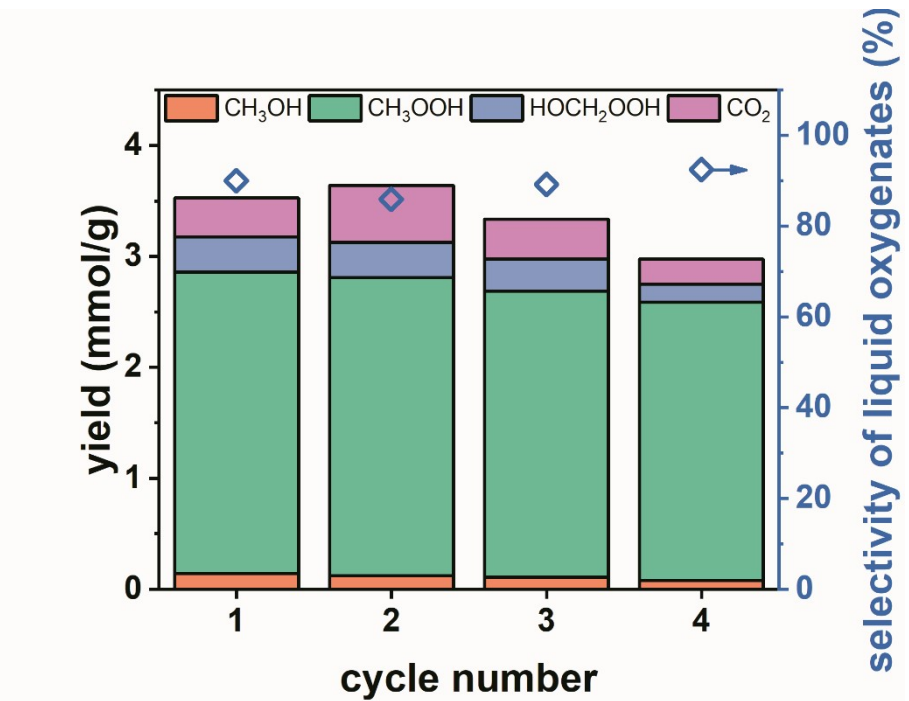
Figure S12. Reuse test of CuNC-600 catalyst. Reaction condition: initial amount of catalyst 5 mg, H_2O 10 mL, reaction time = 0.5 h, 50 °C, $[H_2O_2]$ = 0.5 M, CH_4 28.5 bar, He 1.5 bar.
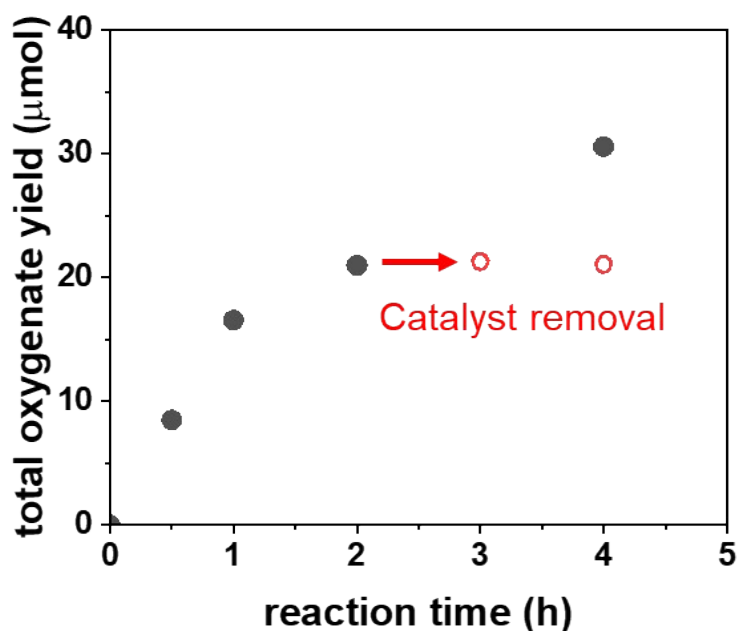
Figure S13. Hot filtration test result.

Reaction condition : CuNC-600 5 mg, H_2O 10 mL, reaction time = 0.5 - 4 h. 40 °C, $[H_2O_2]$ = 0.5 M, CH_4 28.5 bar, He 1.5 bar.

The catalyst was separated from the reaction mixture through filtration after 2 hours, after which 1 mL of the liquid solution was collected for product quantification. Subsequently, the reaction vessel was replenished with methane gas up to 30 bar and the reaction continued for an additional hour. Another 1 mL liquid sample was taken, and the reaction proceeded for a further hour following a recharge of the reaction vessel with methane.
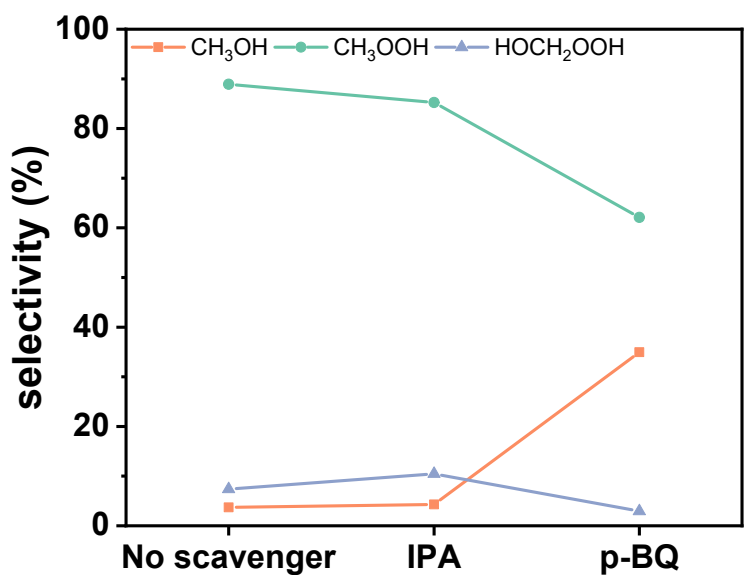
Figure S14. Liquid product selectivity during radical scavenger tests.
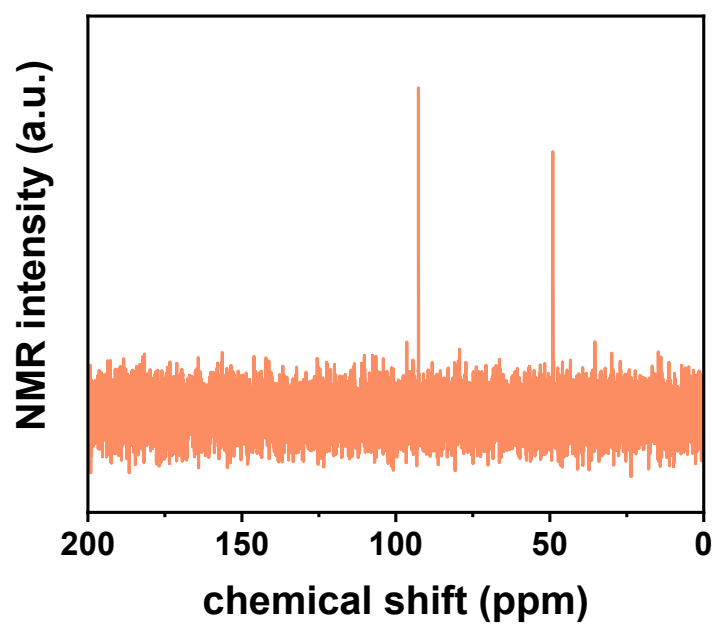
Figure S15. ^{13}C-NMR spectrum of the liquid product after the oxidation of ^{13}CH$_3$OH.

Reaction condition: CuNC-600 5 mg, H$_2$O$_2$ 5 mmol, H$_2$O 10 mL, CH$_4$ 28.5 bar, He 1.5 bar, 40 °C, 1 h.
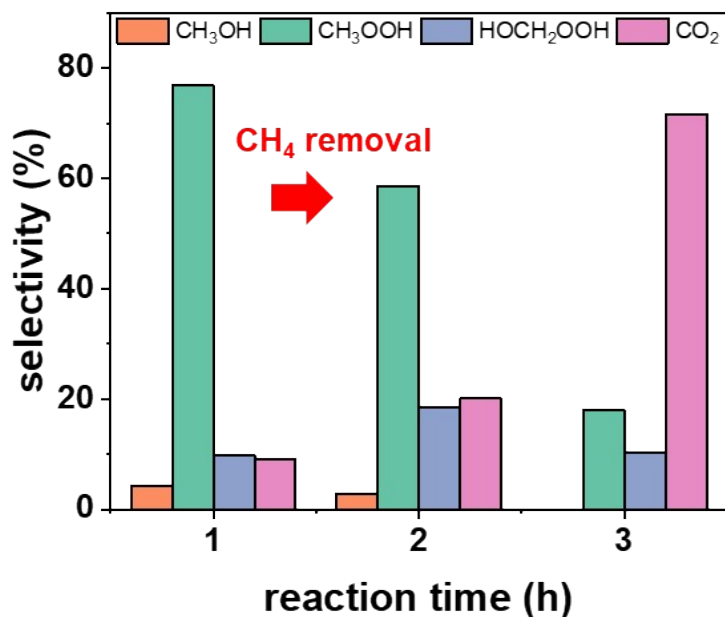
Figure S16. CH_3OOH oxidation result. CH_4 was removed from the reaction vessel after 1 h of reaction under standard conditions. The vessel was re-pressurized to 30 bar with N_2 and the reaction was continued for another 1 and 2 hours.

Table S4. Performances comparison of the thermocatalysts for methane oxidation using H_2O_2.

Catalytic template	Catalyst	Metal-loading (wt%)	Active site structure	P^a (bar)	T^b (℃)	Productivity [µmol / g_{cat} / h]					C1 liquid product selectivity (%)	Turnover Frequency ($mol_{C1\ liquid\ products}$/$mol_{metal}$/h)	Ref.
						CH_3OH	CH_3OOH	$HOCH_2OOH$	$HCOOH$	CO_2			
	CuNC-600	**17.7**	**CuN3**	**30**	**50**	**285**	**5429**	**633**	**0**	**766**	**89.2**	**2.3**	**This work**
Carbon	FeN4/GN	2.7	FeN4	20	25	11	83	63	71	31	88.1	0.34	[S1]
	Cu₁@C₃N₄	0.35	CuN2	30	50	26		0	0	-	-	0.7	[S2]
	Cu₂@C₃N₄	0.35	Cu2O-N4	30	50	260		0	0	16	89.4	4.73	
Metal Oxide	AuPd/TiO₂ (1 wt%)	1	AuPd	30.5	50	76	146	0	0	30	88.1	3.4	[S3]
	Rh/ZrO₂	0.3	Rh₁O₅	30	70	31	7	0	0	10	78	1.7	[S4]
	CuCHA	2.5	-	35	60	13	101	-	-	-	-	0.3	[S5]
	CuFAU	1.1	-	35	60	13	224	-	-	-	-	1.3	
	CuMOR	0.4	-	35	60	6	98	-	-	-	-	1.6	
	CuFER	2.3	-	35	60	104	85	-	-	-	-	0.4	
	CuBEA	1.1	-	35	60	6	126	-	-	-	-	0.7	

[a]Pressure; [b]Temperature.

Table S5. Carbon balance of the reactant and products with time.

t^a (h)	CH_4 consumption (µmol)	Products (µmol)				Carbon balance[b] (%)
		CH_3OH	CH_3OOH	$HOCH_2OOH$	CO_2	
0.5	8.44	0.27	6.46	0.54	1.21	100.5
1	14.85	0.44	11.33	1.19	2.32	102.9
2	19.83	0.74	15.22	1.69	3.16	105.0
4	30.26	0.77	20.87	3.61	5.34	101.1
10	38.42	1.03	15.65	2.46	20.23	102.5
16	47.53	1.59	16.50	2.69	25.65	97.7

[a]Reaction time; [b]Carbon balance = Total yield of the products / CH_4 consumption * 100 %.

Table S6. Reaction rate equations of the proposed reaction equations.

No.	Reaction rate equation	Initial condition
1	$\dfrac{d[CH_4]}{dt} = -k_1[CH_4][H_2O_2] - k_2[CH_4][H_2O_2]^2$	$[CH_4]_0 = 33.8$ mM[a]
2	$\dfrac{d[CH_3OH]}{dt} = k_1[CH_4][H_2O_2] - k_3[CH_3OH][H_2O_2]$	$[CH_3OH]_0 = 0$ mM
3	$\dfrac{d[CH_3OOH]}{dt} = k_2[CH_4][H_2O_2]^2 - k_4[CH_3OOH][H_2$	$[CH_3OOH]_0 = 0$ mM
4	$\dfrac{d[HOCH_2OOH]}{dt} = k_3[CH_3OH][H_2O_2]^2 + k_4[CH_3O$	$[HOCH_2OOH]_0 = 0$ mM
5	$\dfrac{d[CO_2]}{dt} = k_5[CH_3OOH][H_2O_2]^2 + k_6[HOCH_2OOH$	$[CO_2]_0 = 0$ mM

[a]The initial methane concentration was calculated by the interpolation of experimental data provided in the literature.[S6]

Table S7. Best fit results of the reaction rate constants.

Reaction rate constants	
k_1 [$M^{-1}h^{-1}$]	0.0015755
k_2 [$M^{-2}h^{-1}$]	0.1510500
k_3 [$M^{-2}h^{-1}$]	0.0000241
k_4 [$M^{-1}h^{-1}$]	0.5423146
k_5 [$M^{-2}h^{-1}$]	0.0000002
k_6 [$M^{-1}h^{-1}$]	3.015652

References

[S1] Xiaoju Cui, Haobo Li, Yan Wang, Yuanli Hu, Lei Hua, Haiyang Li, Xiuwen Han, Qingfei Liu, Fan Yang, Limin He, Xiaoqi Chen, Qingyun Li, Jianping Xiao, Dehui Deng, and Xinhe Bao, *Chem* **2018**, 4, 1902–1910.

[S2] Pengfei Xie, Jing Ding, Zihao Yao, Tiancheng Pu, Peng Zhang, Zhennan Huang, Canhui Wang, Junlei Zhang, Noah Zecher-Freeman, Han Zong, Dashui Yuan, Shengwei Deng, Reza Shahbazian-Yassar and Chao Wang, *Nat. Commun.* **2022**, 13, 1375.

[S3] Christopher Williams, James H. Carter, Nicholas F. Dummer, Y. Kit Chow, David J. Morgan, Sara Yacob, Pedro Serna, David J. Willock, Randall J. Meyer, Stuart H. Taylor, and Graham J. Hutchings, *ACS Catal.* **2018**, 8, 3, 2567–2576.

[S4] Yongwoo Kwon, Tae Yong Kim, Gihun Kwon, Jongheop Yi, and Hyunjoo Lee, *J. Am. Chem. Soc.* **2017**, 139, 17694−17699.

[S5] Junya Ohyama, Airi Hirayama, Nahoko Kondou, Hiroshi Yoshida, Masato Machida, Shun Nishimura, Kenji Hirai, Itsuki Miyazato and Keisuke Takahashi, *Scientific Reports* **2021**, 11, 2067.

[S6] Jörn Kiepe, Sven Horstmann, Kai Fischer, and Jürgen Gmehling, *Ind. Eng. Chem. Res.* **2003**, 42, 21, 5392–5398